Static and dynamic centrifuge modeling of landslide stabilization with large-diameter shafts

V. Fioravante, D. Giretti, C. Prearo
University of Ferrara, Engineering Department, Via Saragat 1, 44100 Ferrara, Italy

C.G. Lai
University of Pavia, Department of Civil Engineering and Architecture, 27100 Pavia, Italy

SUMMARY
This paper presents the results of a series of static and dynamic centrifuge tests carried out to investigate the stabilisation of shallow landslides by rigid shafts. The experimental campaign was aimed at creating a database on the basis of which calibrating an advanced numerical model to be used as a tool for design.
The centrifuge models reproduced a shallow landslide on a rock slope 32° steep, reinforced by 3.5 m diameter shafts. Three models were tested, both under static and dynamic loading conditions: the unreinforced landslide and the landslide reinforced with one or three aligned piers. During the tests one model shafts was instrumented with strain gauges to measure bending moments.
In the static tests, the shallow landslide was triggered by a displacement-controlled piston which pushed down the top of the slope through a rigid slab which imposed uniform displacements along the slope direction. During the tests the displacements of the sliding mass were monitored through a series of potentiometers. The effect of the insertion of one or three pier was estimated comparing the displacement field of the landslide with and without the reinforcing shafts.
In the dynamic tests a real, properly-scaled time history was applied to the models using a one-degree-of-freedom shaking table installed in the centrifuge. Five accelerometers were embedded into the physical models to measure the seismic excitation and response. The reinforced slope resulted stable under the earthquake loading while the test results clearly showed evidence of ground amplification within the soil mass.

Keywords: landslide, dynamic centrifuge, stabilisation, large diameter shaft

1. INTRODUCTION

Due to its relief and its geomorphological and structural characteristics, Italy is a country in which the landslide risk is particularly high: 470.000 landslides have been reckoned in 20.000 Km^2 (6.8% of national territory) and 5.596 among to 8.101 Italian municipalities are concerned by landslides. The main types of movement are represented by rotational/translational slides, slow earth flows, rapid debris flow and complex landslides. About 45% of the surveyed landslides are classified as active, reactivated or suspended; a significant rate of the total area interested by landslides is affected by shallow sliding phenomena. The triggering mechanisms have mainly morphological, hydrogeological and anthropic nature (ISPRA 2008).
To reduce the risk associated with landslides, various stabilisation methods can be adopted, depending on the type of landslide, the size and speed of the phenomenon, etc. The stabilisation by drilled shafts is a widely accepted practice. Due to the high seismicity of a large part of the Italian territory, any stabilization method has to be designed to withstand to earthquake loading.
With the aim of developing a simplified methodology for the seismic design of landslides stabilisation with large diameter shafts (LDS), the Italian Department of Civil Protection has commissioned to EUCENTRE (European Centre for Training and Research in Earthquake Engineering) a research project which involves the combined use of advanced physical and numerical modelling. The former is aimed to identify the mechanisms controlling the response of a stabilized slope under both static and dynamic loading and to calibrate an advanced numerical model of the system. The latter was aimed at performing parametric analyses at a prototype scale in order to develop a simplified methodology for the design of large diameter shaft systems to reinforce unstable slopes under various geological and geotechnical conditions.

A series of physical tests were performed using a seismic centrifuge. Among the possible types of landslides surveyed in Italy, it was decided to reproduce experimentally a shallow landslide on a rock slope inclined by 32° from the horizontal, reinforced by large diameter shafts well embedded in the firm substratum. The shallow landslides was reproduced using a dry, very fine sand characterised by a shear resistance angle at critical state ϕ'_{cv}=33°. The rock substratum was modelled by a lightweight concrete block. The soil-subsoil interface was rough and produced an interface friction angle, δ' almost equal to ϕ'_{cv}, as it was deduced from interface direct shear tests. The reinforcing LDS were modelled by hollow aluminium alloy cylinders.

Both static and dynamic centrifuge tests were executed with the aim of creating an experimental database for the validation of the numerical model. Three models were tested: the unreinforced landslide and the landslide reinforced with 1 and 3 aligned shafts.

In the static tests the sandy layer representing an unstable, shallow slope was instabilized using a piston that triggered a sliding failure mechanism through a rigid slab imposing a uniform displacement field at the top of the slope. The increment of stability due to the insertion of one or three piers was estimated comparing the displacement field of the sandy layer with and without the reinforcing structures.

In the dynamic tests the models were excited by a one-degree-of-freedom shaking table installed in the geotechnical centrifuge. Monitoring of the tests included measurements of the acceleration time histories within the soil mass and the bending moments of the reinforcing shafts. The input motion was selected as a real and properly scaled accelerogram recorded at the outcropping rock. The ground motion was chosen from a suite of 7 spectrum-compatible records specified for the Garfagnana territory, in Tuscany region, Italy, where the seismic hazard and landslide risk are moderate to high.

This paper presents some of the results of the static and dynamic centrifuge tests performed during the experimental campaign highlighting some peculiar aspects exhibited by the tests.

It is worth recalling the similarity relationships between a centrifuge model and the prototype. In a physical model geometrically scaled by a factor N and subjected to a centrifuge acceleration of Ng, both stresses and strains are scaled 1-to-1. Time in dynamic processes is scaled by a factor N whereas the acceleration is amplified by a factor N (Schofield 1980). The main similarity relationships between physical model and prototype scale are shown in Table 1.

Table 1. Similarity relationships convert quantities from the physical model to a prototype scale.

Quantity	Prototype	Model	Quantity	Prototype	Model
Length, L	N	1	Stress, σ	1	1
Velocity (projectile), v	1	1	Strain, ε	1	1
Acceleration, a	1	N	Mass Density, ρ	1	1
Mass, m	N^3	1	Time (dynamic), t_d	N	1
Force, F	N^2	1	Frequency, f	1	N

2. EXPERIMENTAL SET-UP

The model tests were performed using the ISMGEO (Istituto Sperimentale Modelli Geotecnici, Seriate – BG – Italy) geotechnical centrifuge, herein simply called IGC. The IGC is a beam centrifuge made up of a symmetrical rotating arm with a diameter of 6 m, a height of 2 m and a width of 1 m. The arm holds two swinging platforms, one used to carry the model container and the other the counterweight; during the test, the platforms lock horizontally to the arm to prevent transmitting the working loads to the basket suspensions. An outer fairing covers the arm; the arm and the cover concurrently rotate to reduce air resistance and perturbation during flight; further details can be found in Baldi et al. (1988).

The IGC houses a single degree of freedom shaking table, which is able to reproduce real strong motion events at the model scale. The axis of motion of the shaker is parallel to the centrifuge rotational axis, thus problems related to Coriolis's acceleration and forces are avoided. The shaker is not integrated into the swinging platform, but is directly connected through a rigid arm. At about 5g of acceleration, the platform which holds the model container is moved into contact with the table in flight and released before dynamic excitation starts. The shaker excitation is transferred from the slip table to the model container entirely through mechanical coupling. The shaking table works under an acceleration field up to 100g. It can provide excitations at frequencies up to 500 Hz and acceleration up to 50g.

The adopted geometrical scaling factor of the models was N=50. All the models were tested under an acceleration field of 50g, which was reached in correspondence of the centre of gravity of the model mass.
The centrifuge model reproduced a shallow sandy landslide, 4 m thick, 20 m wide and 22 m long, resting on a rock substratum and reinforced with 1 or 3 large diameter shafts. The sliding surface at the interface between rock and sand was inclined by 32° to the horizontal.
Three static and three dynamic tests were performed and three models were tested: the unreinforced sandy landslide (tests T0.S – static – and T0.D – dynamic) and the landslide reinforced with 1, central (tests T1.S and T1.D) and 3, aligned shafts (tests T3.S and T3.D). The model and the prototype geometrical dimensions are listed in Table 2. Figures 1 and 2 show the general layout of the static and dynamic tests, respectively (all measures refer to the model scale). The rock slope was modelled through a light-weight concrete block fixed to the centrifuge strong box (shear wave velocity $V_S \approx 950$ m/s as deduced with reference to linear elasticity from the Young's modulus and Poisson's ratio measured in uniaxial cylindrical tests with local strain measurements). The sandy landslide was modelled by a very fine and uniform silica powder, derived by grinding and sieving pit rocks, named FF sand (FFS). It mainly consists of sub angular particles and it is made of 98.2% quartz, 1.3% feldspar and 0.5% mica. The main characteristic of FFS are: maximum and minimum dry density, $\gamma_{d,max}$ = 14.78 kN/m^3, $\gamma_{d,min}$ =11.58 kN/m^3; maximum and minimum void ratio, e_{max} = 1.211, e_{min} = 0.732; specific density, G_S = 2.61; mean particle size, D_{50} = 0.093 mm; uniformity coefficient, U_C = 1.88. The critical state parameters are: shearing resistance angle at critical state, ϕ'_{cv} = 33°; critical stress ratio, M = 1.35; void ratio at p'= 1 kPa, e_Γ = 1.15; slope of the critical state line in the e-ln(p') plane, λ = 0.026. The sand layer was reconstituted by tamping the sand, with a moisture content of 5%, in four horizontal layers 20 mm thick, having inclined the box -32° to the horizontal, so that the strata were parallel to the rock slope. The average relative density achieved at the end of the 50g in–flight consolidation was $D_R \approx 40\%$. The soil-concrete interface was rough and produced an interface friction angle, δ' equal to ϕ'_{cv}, as deduced from several interface direct shear tests. The model container was designed with rigid walls to confine the model in the y direction, perpendicular to the shaking axis, x (Figs. 1 and 2). The side friction between the soil and the container walls was minimised by lubricating the lateral surfaces. The reinforcing shafts were modelled by 70 mm external diameter, D_e (3.5 m at the prototype scale) aluminium alloy cylinders. The shaft spacing in the tests with 3 reinforcing piers was equal to $1.5D_e$ = 105 mm (5.25 m at the prototype scale). The thickness of the cylinder was chosen to properly scale the flexural rigidity of the shaft: $(E_p\, I_p) = N^4(E_m\, I_m)$ (see Fioravante, 2008). Referring to a prototype concrete shaft (E_p = 35 GPa) with an external diameter of 3.5 m and an internal diameter of about 2.6 m (I_p = 5.12 m^4), the prototype flexural rigidity is $E_p\, I_p$ = 179 GNm^2. Since the aluminium alloy has E_m = 70 GPa, the inertia moment $I_m = 4.1\cdot10^{-7}$ m^4 can be reproduced by a hollow cylindrical solid with external diameter of 70 mm and internal diameter 63 mm. One model pier (shaft 1 in Figs. 1 and 2) was instrumented with 5 pairs of strain gauges, as shown in Figure 3, to measure the induced bending moments of the shaft at various height. The strain gauges were glued to the external surface and properly calibrated. Each model was prepared at 1g, then it was embarked into the centrifuge, accelerated to 50g and allowed to consolidate due to the self-weight. In the static tests the landslide was triggered by a displacement-controlled piston which pushed down the top of the slope through a rigid slab connected to a hydraulic actuator which imposed a displacement field (Figure 1). The raft was allowed to slide parallel to the slip interface and produced a uniform displacement field. The force applied by the actuator was gradually increased up to the sliding condition was reached.

Table 2. Geometrical dimensions at the model and the prototype scale.

	Dimension	Model scale [mm]	Prototype scale [m]
Sand landslide	thickness, t	80	4
	Elevation	235	11.75
	Length, L	444	22.2
	slope, i	32°	
Shaft	external diameter, D_e	70	3.5
	high, H	200	10
	average embedment, b	80.4	4
	shaft spacing, s (s/D_e =1.5)	105	5.25

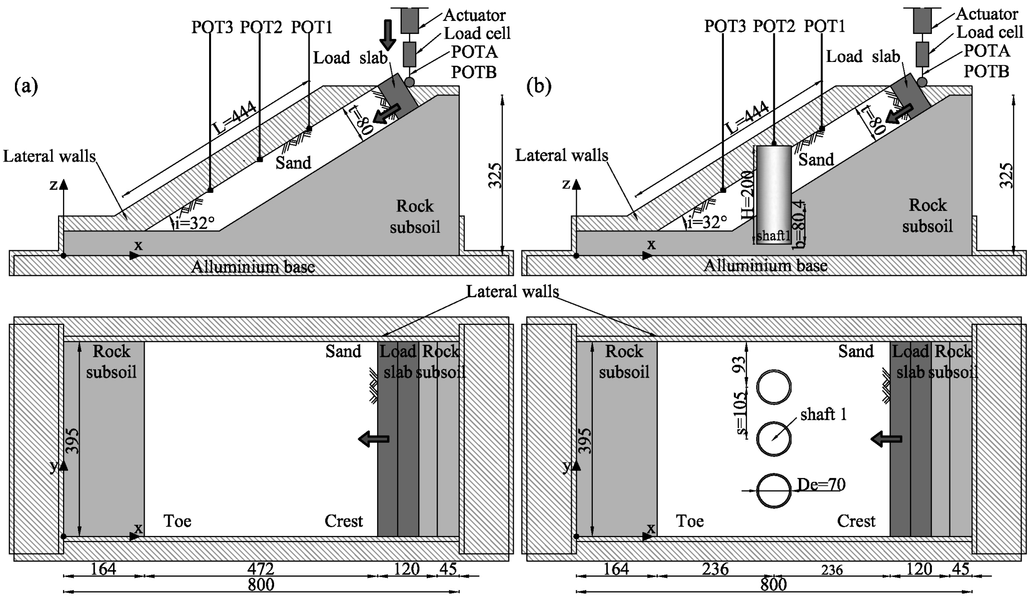

Figure 1. Layout of the static tests (model scale): cross section and plane view of (a) the unreinforced model, (b) the reinforced model. All dimensions are in mm.

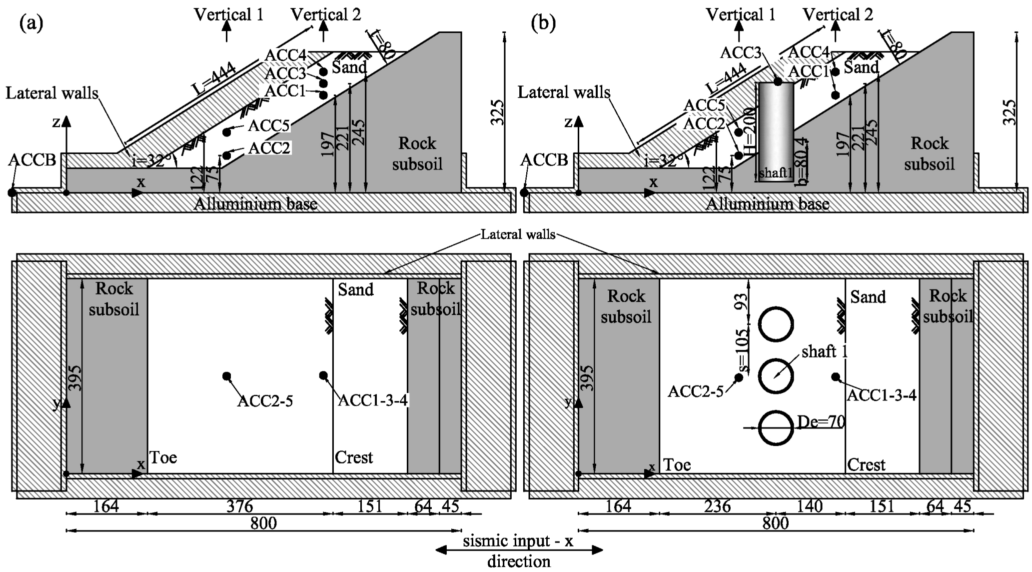

Figure 2. Layout of the dynamic tests (model scale): cross section and plane of (a) the unreinforced model, (b) the stabilised model. All dimensions are in mm.

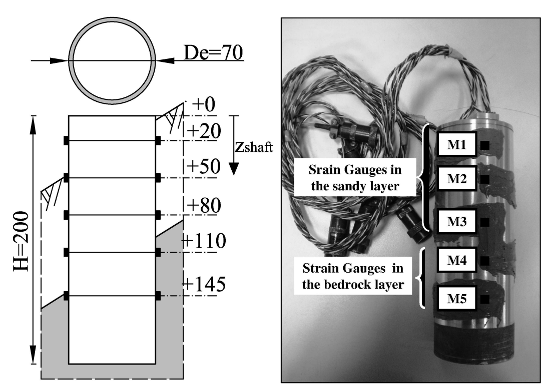

Figure 3. Shaft model (model scale). All dimensions are in mm.

In the dynamic tests the models were excited by a one-degree of freedom shaking table installed into the centrifuge. As input motion a real, properly scaled accelerogram recorded on outcropping rock was used. The motion was selected from a set of 7 spectrum-compatible spectrum specified for Garfagnana territory, in Tuscany region, Italy (Lai et al. 2008). The time history of acceleration and the pseudo-acceleration spectrum of the input motion are represented in Figure 4 (a) and (b), respectively. The main characteristics of the motion are given in Table 3, where PGA, PGV and PGD = peak ground acceleration, velocity and displacement; d_{90} = significant duration; I_A = Arias Intensity and s = Housner Spectrum Intensity evaluated on the pseudo-acceleration spectrum PSA. The peak acceleration is PGA = 0.178g; the predominant period is 0.1 s. In the static tests (Figure 1) the instrumentation consisted of:

- N. 3 vertical displacement and rotational transducers to measure the sliding mass displacements along the centre line of the model at three target points: the first placed at the upper portion of the slope (POT1), the second at mid-height or alternatively at the top of the reinforcing shaft (POT2), the third at the lower portion of the slope (POT3);
- N. 1 loading cell to measure the load applied to the slab;
- N. 2 vertical displacement transducers (POTA, POTB) to measure the slab displacements.

The quantities measured by the instruments were recorded at a frequency of 1 Hz.
In the dynamic tests (Figure 2) the instrumentation consisted of:

- N. 5 accelerometers to measure the accelerations along the centre line of the model: ACC1 and 4 in the upper portion of the sliding mass - vertical 1; ACC2 and 5 in the lower portion of the sliding mass - vertical 2.; the accelerometer ACC3 was placed between ACC1 and 4 in the model without the reinforcing shafts, or at the top of the centre pier in the reinforced models; the accelerometers were arrange to measure acceleration in the x direction;
- N. 1 accelerometer to measure the acceleration in the x direction at the rigid base of the model (ACCB).

The quantities measured by the instruments were recorded at a frequency of 5000 Hz.

3. STATIC TEST RESULTS

All the results discussed hereinafter are referred to the prototype scale; T0.S (unreinforced slope) is assumed as reference test.
Figures 5, 6 and 7 report the results of the tests T0.S, T1.S, T3.S, respectively. In these Figures, ξ is the direction of the slope. The displacements of the sand landslide at the target points measured by the potentiometers (POT1, POT2, POT3) and projected along ξ, $R_{i,\xi}$, (i = 1, 2, 3) are plotted against of the displacement imposed by the slab in the ξ direction, $R_{slab,\xi}$. The $R_{i,\xi}$ values are plotted at a semi-log scale to amplify the first part of the curves.
As to the unreinforced landslide (Figure 5), the displacements of the sand are small up to a slab settlement $R_{slab,\xi} \approx 40$ cm, after which a pronounced knee can be observed and the displacements start to increase with a greater gradient at the crest than at the toe.

Table 3. Characteristic of the input motion. Prototype scale.

PGA [g]	PGV [g·s]	PGD [g·s^2]	d_{90} [s]	$I_{a,max}$ [g·s]	$s_{(0.1\text{-}0.5)}$ [m]	$s_{(0.5\text{-}1.5)}$ [m]
0.178	0.167	0.073	29.17	0.008	0.172	0.121

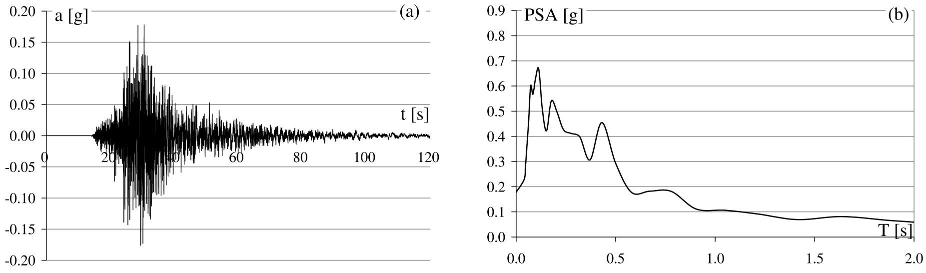

Figure 4. Input motion of the dynamic tests: (a) time history of accelerations; (b) pseudo-acceleration spectrum. Prototype scale.

In the slope reinforced with 1 pier (test T1.S, see Fig. 6), the sand movements are concentrated upstream of the shaft: the displacements measured by POT3 are negligible, while those measured by POT1 increase at a significant rate after a slab displacement $R_{slab,\xi} \approx 50$ cm. The sand displacements cause a modest displacement of the top of the pier, lower than 3.2 cm, as measured by POT2. Similar results have been obtained by the test with 3 reinforcing shafts (T3.S, see Figure 7); the sand at the upstream starts to move significantly in correspondence of a slab displacement $R_{slab,\xi} \approx 60$ cm, causing a displacement of the top of the piers lower than 1.5 cm. The effects of the displacements of the slab at the crest do not propagate downstream of the piers.

If the slab displacements $R_{slab,\xi} = 40$, 50 and 60 cm are assumed as the displacements which trigger large plastic deformations of the sand landslide (sliding), the reinforcing effect of the shafts can be evaluated in terms of increment of the "sliding threshold", i.e. increment of the slab displacement required to trigger the sliding of the sandy layer. These increments can be quantified as follows: $(R_{slab,\xi})_{T1.S}/(R_{slab,\xi})_{T0.S} = 50/40 = 1.25$ and $(R_{slab,\xi})_{T3.S}/(R_{slab,\xi})_{T0.S} = 60/40 = 1.5$.

This reinforcing effect of the shafts is graphically represented by Figures 8 and 9. Figure 8 sketches the resultant vectors, R_i of the displacements of the target points measured by POT1, 2, 3 for all the three tests T0.S, T1.S and T3.S: the ξ axes represents the free surface of the slope in its un-deformed configuration. Each vectors is subdivided in two parts: the first from the beginning of the test up to the triggering of the sliding, the second from the sliding condition up to a displacement imposed by the slab equal to 100 cm. The insertion of 1 and 3 piers yields: i) a drastic reduction of the movement of the sand at the downstream of the hafts, as measured by POT3; ii) a significant decrease of the displacements at the upstream (POT1), and iii) the increment of the sliding threshold. In the unreinforced slope the target point at the crest moves almost parallel to the slope direction, while in presence of the piers it tends to move almost horizontally. In Figure 9, the displacements $R_{1,\xi}$, $R_{2,\xi}$ and $R_{3,\xi}$, measured in correspondence of three values of the displacement imposed by the raft, $R_{slab,\xi} = 25$, 50 and 100 cm are compared for tests T0.S, T1.S and T3.S. The effect of the shafts in reducing the sand displacements is shown.

In Figure 10 two pictures taken at the end of the tests T.1S and T3.S are shown. They evidence the failure surfaces and the soil flowed around the piers. The presence of three shafts concentrates the soil deformations upstream.

The values of the bending moment measured at $R_{slab,\xi} = 100$ cm by the strain gauges attached on shaft 1 during the tests T1.S and T3.S are plotted in Figure 11 as a function of the distance from the top of the shaft.

In the Figure are also shown the values of the bending moment at the end of the in-flight consolidation, which are due to the earth pressure at rest. The maximum moment always occurs in correspondence of the sand-rock interface and it is about 3 times higher than that due the earth pressure at rest. This is due to the partial mobilisation of the passive resistance of the soil mass pushed down toward the piers. The centre pier of T3.S has slightly lower bending moments than the single pier of T1.S, consistently to the lower top displacement.

4. DYNAMIC TEST RESULTS

The pseudo-acceleration spectra PSA of the motions measured during the tests T0.D, T1.D, T3.D are plotted at the prototype scale in the Figures 12, 13 and 14. In each Figure the PSA of the applied earthquake, measured by the accelerometer ACCB (at the rigid substratum), is compared with the PSA of the record measured within the sand downstream (ACC5) and upstream (ACC4). On the Figures are also reported the amplification factors FA and FH, computed with eqs. 1-4, and the main characteristics of the measured motions.

$$FA_{0.1\text{-}0.5} = \frac{s_{0.1\text{-}0.5}(PSA_{ACCi})}{s_{0.1\text{-}0.5}(PSA_{ACCB})} \quad (1) \qquad FA_{0.5\text{-}1.5} = \frac{s_{0.5\text{-}1.5}(PSA_{ACCi})}{s_{0.5\text{-}1.5}(PSA_{ACCB})} \quad (2)$$

$$FH_{0.1\text{-}0.5} = \frac{s_{0.1\text{-}0.5}(PSV_{ACCi})}{s_{0.1\text{-}0.5}(PSV_{ACCB})} \quad (3) \qquad FH_{0.5\text{-}1.5} = \frac{s_{0.5\text{-}1.5}(PSV_{ACCi})}{s_{0.5\text{-}1.5}(PSV_{ACCB})} \quad (4)$$

where: i = 4, 5; $s_{0.1\text{-}0.5}$ = is the Housner intensity of the pseudo-acceleration (or pseudo-velocity) spectrum between the periods 0.1 s – 0.5 s; $s_{0.5\text{-}1.5}$ = is the Housner intensity of pseudo-acceleration (or pseudo-velocity) spectrum between the periods 0.5 s – 1.5 s.
The earthquakes applied by the shaking table in the dynamic tests slightly differ each other and from the reference motion (see Table 3 and Figure 4). Despite of these differences, the test results indicate the tendency of the sandy layer to amplify the input motion especially in the range of periods from 0.1 to 0.5 s.
In the tests without reinforcing shafts the amplification phenomena are larger upstream than downstream, possibly due to the focalisation of the seismic waves near the crest. Despite of the significant amplification of the motion within the sand layer, the slope is stable during shaking and no sliding surface were recorded at the end the tests. This is confirmed by the distribution of excess bending moments of the shaft, respect to the values at rest, shown in Figure 15, where the measured moments are plotted as a function of the distance from the top of the pier. During shaking the shaft experiences only a small increment of the bending, i.e. the earth pressure increment is modest. The shaft behaves like a single degree of freedom system with a natural period T_n = 0.12 s, very close to the predominant period of the input motions (0.1 s). As a matter of fact the shaft experiences significant amplification of the input motion as shown in Figure 16 where the response spectra of the acceleration at the top of shaft 1 measured in the tests T1.D and T3.D are compared. A peak amplification of 2.3-3 at T_n = 0.12 s can be observed.

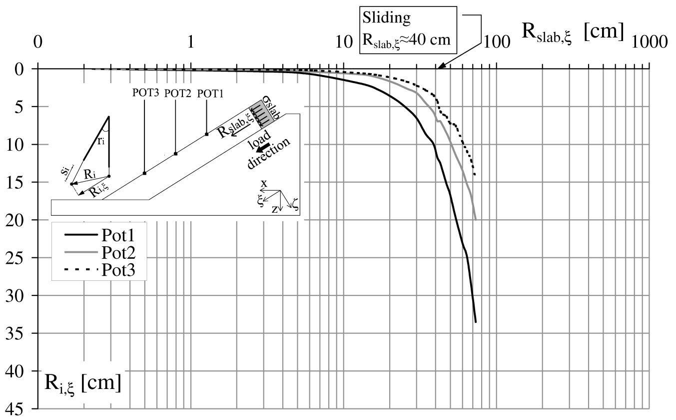

Figure 5. Test T0.S: displacement of the measuring points vs. of the displacement of the slab (values projected in the direction of the slope, ξ).

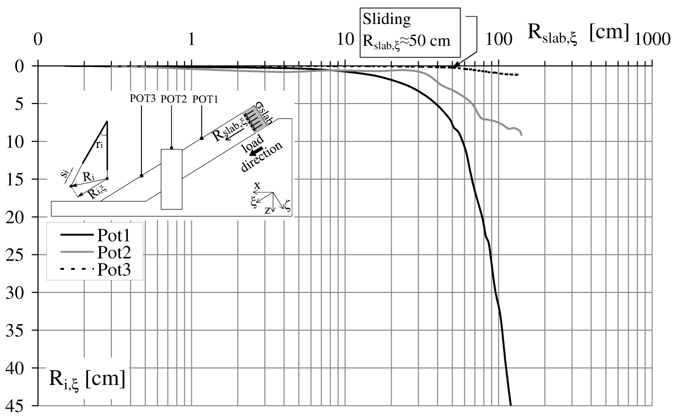

Figure 6. Test T1.S: displacement of the measuring points vs. of the displacement of the slab (values projected in the direction of the slope, ξ).

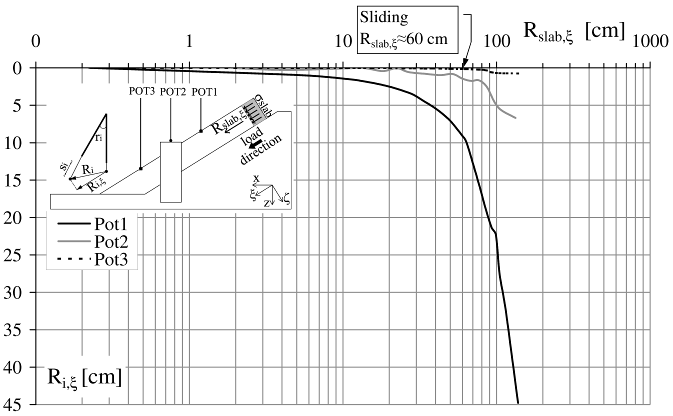

Figure 7. Test T3.S: displacement of the measuring points vs. of the displacement of the slab (values projected in the direction of the slope, ξ).

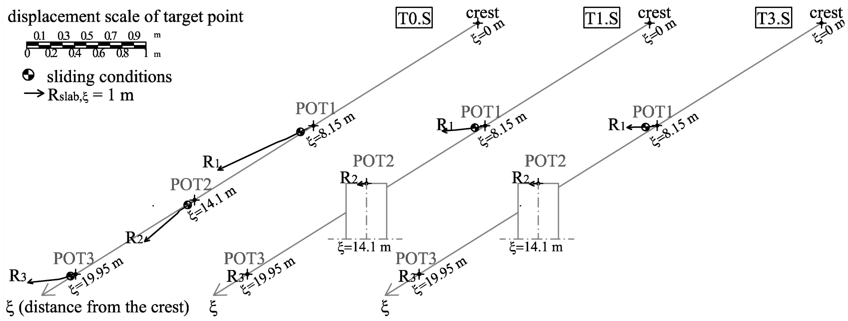

Figure 8. Tests T0.S-T1.S-T3.S: resultant of the measured displacements.

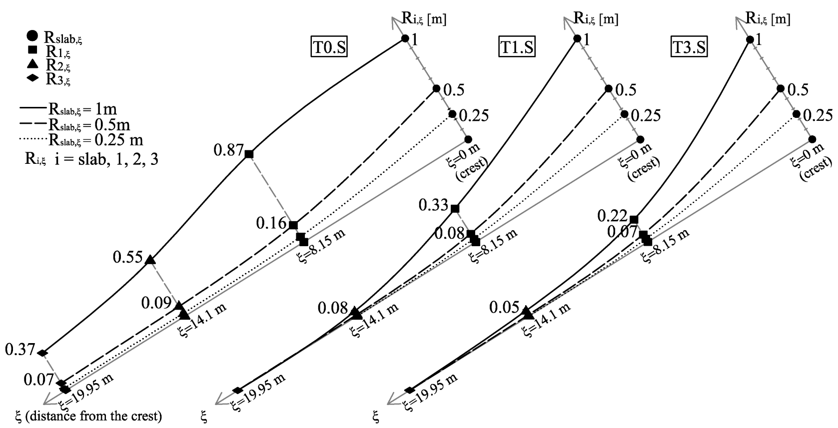

Figure 9. Tests T0.S-T1.S-T3.S: normalised displacements in the direction of the slope, ξ.

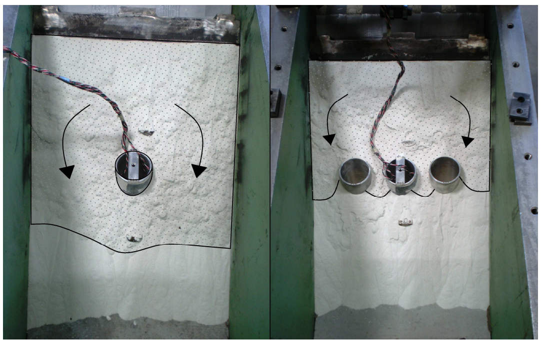

Figure 10. Tests T1.S-T3.S: pictures of the failure surfaces.

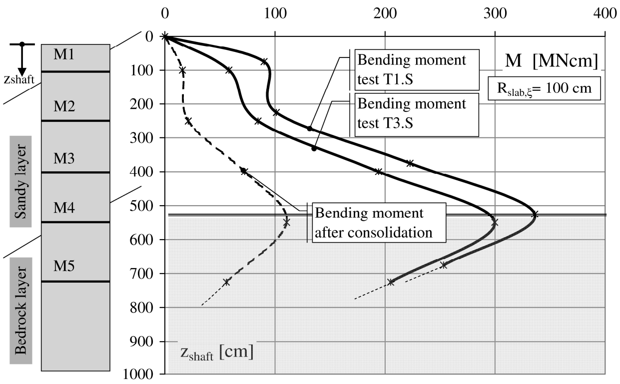

Figure 11. Tests T1.S and T3.S: values of the bending moment measured on shaft 1.

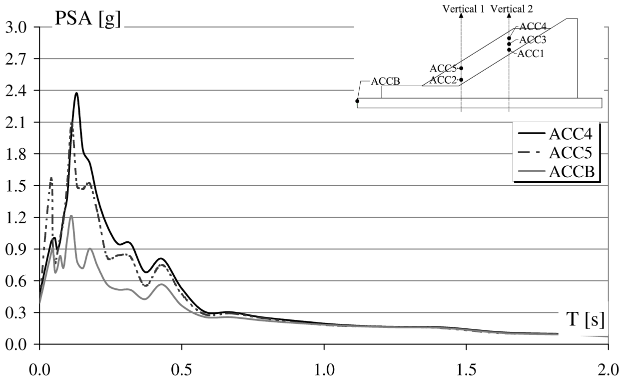

		base	toe	crest
		ACCB	**ACC5**	**ACC4**
PGA	[g]	0.392	0.411	0.474
d90	[s]	52.03	77.59	82.12
Pd,90	[$g\cdot s^3\cdot 10^{-4}$]	1.12	3.11	6.91
Ia,max	[g·s]	0.03	0.13	0.23

	toe		crest	
ΔT [s]	FA [-]	FH [-]	FA [-]	FH [-]
0.1 - 0.5	1.50	1.58	1.74	1.85
0.5 - 1.5	1.05	1.07	1.10	1.13

Figure 12. Test T0.D: pseudo-acceleration response spectra.

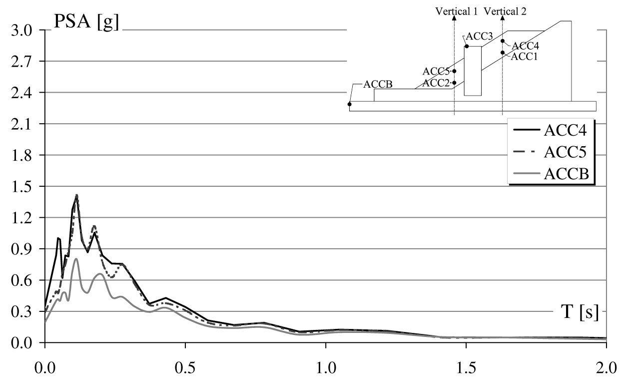

		base	toe	crest
		ACCB	**ACC5**	**ACC4**
PGA	[g]	0.194	0.294	0.351
d90	[s]	24.35	45.72	58.56
Pd,90	[$g\cdot s^3\cdot 10^{-4}$]	0.25	0.92	1.57
Ia,max	[g·s]	0.01	0.04	0.05

	toe		crest	
ΔT [s]	FA [-]	FH [-]	FA [-]	FH [-]
0.1 - 0.5	1.43	1.51	1.51	1.58
0.5 - 1.5	1.19	1.21	1.12	1.28

Figure 13. Test T1.D: pseudo-acceleration response spectra.

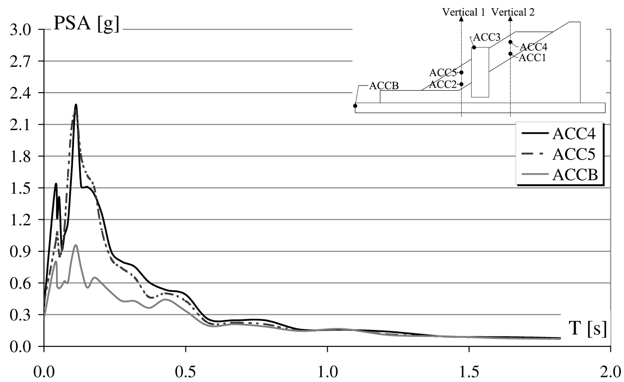

		base	toe	crest
		ACCB	**ACC5**	**ACC4**
PGA	[g]	0.269	0.418	0.377
d90	[s]	50.27	72.33	79.57
Pd,90	[$g\cdot s^3\cdot 10^{-4}$]	0.65	2.41	3.34
Ia,max	[g·s]	0.02	0.15	0.16

	toe		crest	
ΔT [s]	FA [-]	FH [-]	FA [-]	FH [-]
0.1 - 0.5	1.59	1.80	1.72	1.87
0.5 - 1.5	1.05	1.07	1.16	1.19

Figure 14. Test T3.D: pseudo-acceleration response spectra.

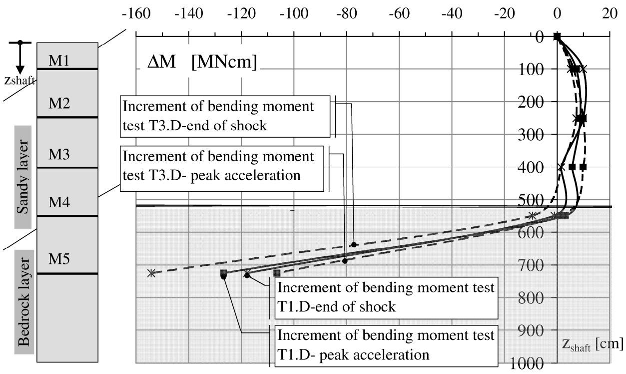

Figure 15. Tests T1.D and T3.D: bending moment measured on shaft 1 during shaking (maximum acceleration) and at the end of tests.

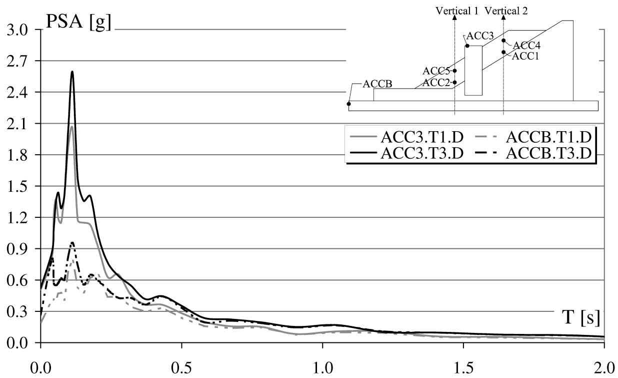

		T1.D		T3.D	
		ACCB	ACC3	ACCB	ACC3
PGA	[g]	0.194	0.505	0.269	0.523
d90	[s]	24.35	35.77	50.27	57.03
Pd,90	[$g\cdot s^3\cdot 10^{-4}$]	0.25	1.04	0.65	1.39
Ia,max	[g·s]	0.01	0.04	0.02	0.09

	T1.D		T3.D	
ΔT [s]	FA [-]	FH [-]	FA [-]	FH [-]
0.1 - 0.5	1.44	1.62	1.42	1.65
0.5 - 1.5	1.12	1.13	1.03	1.04

Figure 16. Tests T1.D and T3.D: pseudo-acceleration response spectra at the top of shaft 1.

5. CONCLUSIONS

This paper presented some of the results of centrifuge tests performed to investigate the stabilisation of shallow landslides by rigid shafts. The experiments were aimed at identifying the mechanisms controlling the response of a stabilized slope under both static and dynamic loading and to calibrate an advanced numerical model of the system. The numerical simulations are ongoing and are conducted using the finite difference-based solver FLAC^{2D}. Some preliminary results of the numerical simulations of the experiments are given in a companion paper.

ACKNOWLEDGMENTS

The authors would like to express their gratitude to the Italian Department of Civil Protection of Italian Government and EUCENTRE, for having funded the research project (Progetto Esecutivo 2009-2012 – No. e6) and the ISMGEO staff for the assistance during the experimental working campaign, specifically Mr. Sergio Airoldi for his tireless dedication and competence.

REFERENCES

Baldi, G., Belloni, G., Maggioni, W. 1988. The ISMES Geotechnical Centrifuge. In Centrifuge 88, Paris, Corté J. F. Ed., Balkema, Rotterdam, pp. 45-48.

Fioravante (2008) “Physical modelling of landslide stabilization methods in an overconsolidated clay”, Geotechnical testing journal, vol 31, no. 2, pp. 175-191.

ISPRA (2008). Landslide in Italy, Special Report.

Lai, G.C., Strobbia, C., Dall’Ara, A. (2008). Definizione dell’input sismico nei territori toscani della Lunigiana e Garfagnana. Rivista Italiana di Geotecnica, Vol.1/08, pp.9-29

Schofield, A.N. 1980. Cambridge Geotechnical Centrifuge Operations. Geotechnique, Vol. 24, No. 4, pp. 227-268.